Optics Letters

Instantaneous frequency measurement of dissipative soliton resonant light pulses

C. Cuadrado-Laborde,[1,2,3,*] I. Armas-Rivera,[4] A. Carrascosa,[1] E. A. Kuzin,[5] G. Beltrán-Pérez,[4] A. Díez,[1] and M. V. Andrés[1]

[1]Departamento de Física Aplicada y Electromagnetismo, ICMUV, Universidad de Valencia, C/Dr. Moliner, 50, Burjassot 46100, Spain
[2]Instituto de Física Rosario (CONICET-UNR), Blvr. 27 de Febrero 210bis, S2000EZP Rosario, Santa Fe, Argentina
[3]Pontificia Universidad Católica Argentina, Facultad de Química e Ingeniería, Av. Pellegrini 3314, 2000 Rosario, Argentina
[4]Benemérita Universidad Autónoma de Puebla, Facultad de Ciencias Físico Matemáticas, Avenida San Claudio y 18 Sur, Col. San Manuel CU, Puebla 72570, Mexico
[5]INAOE, Enrique Erro 1, Tonantzintla, Puebla, Pue. 72000, Mexico
*Corresponding author: christian.cuadrado@uv.es

We measured the instantaneous frequency profile of two different dissipative soliton resonant (DSR) light pulses, the usual flat-top and less-common trapezoid-shaped light pulses. The DSR light pulses were provided by an ytterbium-doped polarization-maintaining fiber ring passively mode-locked laser using the adequately selected amount of net-normal dispersion. We confirmed that the DSR light pulses have a (moderately) low linear chirp across the pulse, except at the edges, where the chirp changes exponentially. This unique instantaneous frequency behavior can be succinctly resumed by the following parameters: linear chirp slope and leading and trailing chirp lifetimes. As the pump power increases, the linear chirp slope decreases, whereas the leading and trailing chirp lifetimes do not show an appreciable change. The results are compared with previous theoretical works. © 2016 Optical Society of America

Recently, a new soliton formation named *dissipative soliton resonance* (DSR) has attracted considerable attention within the field of mode-locked lasers as it circumvents pulse breaking. Under the DSR regime, with increasing pump power the pulse clamps its peak power while it keeps broadening in the time domain. Evidently, DSR shows great potential for extremely high-pulse energy generation. From a theoretical point of view, DSR are stable solutions of the complex cubic-quintic Ginzburg–Landau equation (CQGLE) [1,2]. There are six coefficients in the CQGLE representing attenuation, bandwidth of a spectral filter, high-order Kerr nonlinearity, dispersion, nonlinear amplification, and saturation of nonlinear amplification. Stable solutions were found by fixing four of them, while varying dispersion and nonlinear amplification. It was numerically shown that a solution of the DSR type occurs when dispersion and nonlinear amplification are located on a special area in the dispersion-nonlinear amplification space. As expected, the resonance curve in the dispersion-nonlinear amplification space depends strongly on the choice of the remaining system's parameters. Also, it is important to realize that unlike conventional soliton solutions, which only exist in the anomalous dispersion regime, DSR is possible in both anomalous and normal dispersion regimes [3]. Experimentally, DSR emission was proven in a myriad of different laser cavities using different mode lockers for both normal and anomalous dispersion [4–10]. Very recently, we developed a DSR mode-locked laser, where, for the first time, the polarization state within the cavity is well defined [11]. Although, it is clear that a lot of experimental progress has been reached in the generation of DSR light pulses, much less progress has been gained in the knowledge of its phase profile or its first-order time derivative, i.e., the instantaneous frequency profile. The necessity of this investigation is clear since the behavior of a light pulse is highly influenced by its temporal phase profile. Theoretically, a linear chirp across the pulse and a much more rapidly varying chirp at the edges has been predicted [3,12,13]. However, as far as we know, no experimental evidence has been provided to date.

In this work, we measured the instantaneous frequency profile of DSR light pulses under two different dispersion values. The DSR light pulses were provided by an ytterbium-doped polarization-maintaining fiber ring passively mode-locked laser that we previously developed [11]. This laser generates two different kinds of DSR light pulses as the net-normal dispersion increases, standard square-shaped flat-top and less-usual right-angle trapezoid-shaped light pulses. In both cases, the instantaneous frequency profile was measured as a function of the pump power. The measured chirp profiles follow the general trend previously reported in theoretical works [3,12,13].

The DSR light pulses under analysis were provided by an ytterbium-doped fiber ring passively mode-locked laser. A semiconductor saturable absorber mirror (SESAM) was used as a
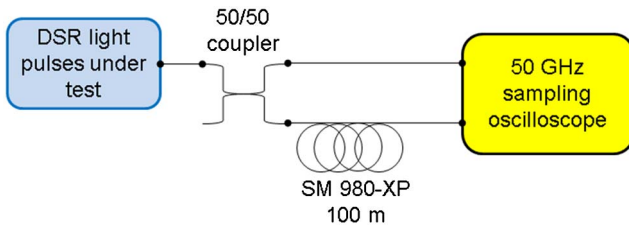
Fig. 1. Experimental setup to retrieve the instantaneous frequency profile of the DSR light pulses.

Fig. 2. (a) Measured intensity profile of a flat-top square-shaped DSR light pulse when the pump power was 583 mW together with its corresponding fitting, solid curve and open scatter points, respectively. The same pulse after propagation by a 100 m long optical fiber dispersive line is also shown (dotted curve). (b) Measured instantaneous frequency profile together with its corresponding fitting, solid curve and solid crosses, respectively, corresponding to the pulse on the left.

mode locker, whereas the polarization was preserved along the whole length of the laser cavity by using polarization-maintaining (PM) optical fibers and components. This laser provides the typically square-shaped flat-top DSR light pulses with a time width in the range of 50–280 ps for a pump power range of 293 mW–583 mW, respectively, at the emission wavelength of 1040 nm. The laser operates in the net-normal dispersion regime with a total cavity dispersion of 8×10^{-3} ps^2. Further details and characterization of this laser can be found in Ref. [11]. With regard to the optical fiber dispersion technique used to retrieve the instantaneous frequency profile, a 100 m long SM 980-XP optical fiber was used as the dispersive line (Nufern, numerical aperture 0.200, dispersion parameter –42 ps/nm × km at the emission wavelength). The technique requires only the measurement of the temporal intensity profile at the input and output of the dispersive line together with the knowledge of the chromatic dispersion of the optical fiber, see Fig. 1. Then, the instantaneous frequency profile is obtained by using just a single equation in a non-iterative single-step numerical calculation. Further details of this technique can be found in Refs. [14,15]. It is worthwhile to point out that this technique is particularly well suited for relatively long pulses that can be accurately recorded using currently available oscilloscopes.

There have been previous attempts to describe DSR light pulses with different analytical functions [3]. However, they hardly provide the necessary steepness and flat-top characteristics of experimentally measured temporal DSR profiles. On the contrary, we found that DSR light pulses are best fitted with a super-Gaussian temporal waveform, whose field envelope can be described as

$$f(t) = \exp\left(-\frac{1}{2}\left(\frac{t}{T_0}\right)^{2m}\right), \qquad (1)$$

where $m \in N$ controls the degree of edge sharpness, and T_0 is a time-width parameter; which in turn can be related to the 10%–90% intensity rise time (T_r) through $T_r = \ln(9)T_0/2\,m$ [16]. Figure 2(a) shows, as an example, the measured temporal intensity profile for a pump power of 583 mW together with the proposed fit according to Eq. (1) with $m = 10$. As it can be observed, the proposed waveform completely overlaps the experimental data. The same figure also shows the dispersed input pulse after propagation by the 100 m long optical fiber. With both temporal intensity profiles, the instantaneous frequency is recovered according to the procedure developed in Refs. [14,15]. On the other hand, Fig. 2(b) shows the measured instantaneous frequency profile recovered by using the optical fiber dispersion technique [14,15]. The pulse dynamics shown in Fig. 2(b) confirm all the essential
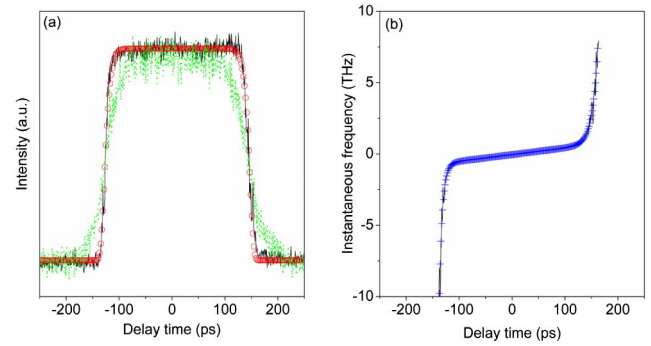
features previously predicted by different theoretical works under normal dispersion [3,12]. It includes the nonzero linear frequency chirp across the pulse profile as well as the exponential chirp at the edges. We found that it can be adequately fitted with the following function:

$$\nu(t) = kt + a_t \exp\left(\frac{t}{T_t}\right) - a_l \exp\left(-\frac{t}{T_l}\right), \qquad (2)$$

where T_l and T_t are the chirp lifetimes of the leading and trailing edges; whereas a_l and a_t are their corresponding amplitude constants, and k is the linear chirp slope. One advantage of Eq. (2) is that it is not piecewise defined, but continuously differentiable over its whole domain. In this way, it can be incorporated as a trial function, or ansatz, for further theoretical research. The corresponding instantaneous frequency fitting following Eq. (2) can also be observed in Fig. 2(b). The degree of resemblance between both experimental and fitted function is remarkable, being essentially indistinguishable between them. The instantaneous frequency profile across the DSR light pulse presents a moderately low linear chirp at the rate of 5 GHz/ps. However, at both leading and trailing edges the instantaneous frequency changes exponentially but with different lifetimes (6 and 10 ps for the leading and trailing chirp lifetimes, respectively).

One distinctive feature of DSR is its behavior as the pump power changes. It has been demonstrated through both theoretical and experimental work [1,11] that DSR light pulses increases their temporal width as the pump power increases, while the peak power and the spectral width remain practically constant. In this sense, it would be desirable to know how the instantaneous frequency profile changes as the pump power varies. Figure 3 shows the result of this experiment for a pump power excursion from 293 to 583 mW. The lower limit represents the pump power threshold for self-started mode locking, whereas the upper limit of the pump power is limited only by the available capability of the source. The main parameters of fitting according to Eq. (2), the linear chirp slope and leading and trailing chirp lifetimes, can be found in Table 1 (for clarity, the curves corresponding to these fittings are not shown in
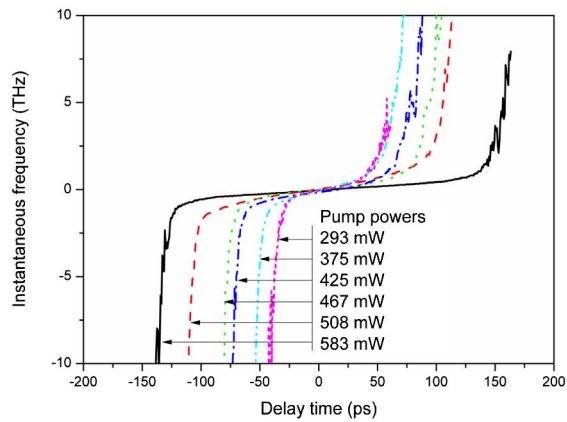
Fig. 3. Measured instantaneous frequency profiles for different pump powers for flat-top square-shaped DSR emission.
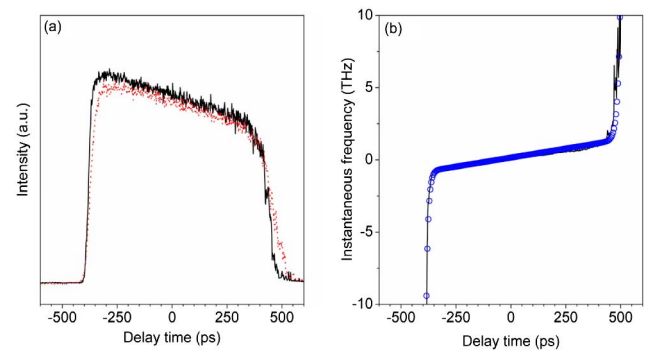

Fig. 4. (a) Measured intensity profile of a trapezoid-shaped DSR light pulse for the pump power of 577 mW, together with the same pulse after propagation by a 90 m long optical fiber dispersive line (solid and dashed curves, respectively). (b) Measured instantaneous frequency profile together with its corresponding fitting, solid curve and open scatter points, respectively, corresponding to the pulse on the left.

Fig. 3). It can be observed in Fig. 3 that the slope of the linear frequency chirp across the pulse profile changes as the pump power varies. On the other hand, leading and trailing chirp lifetimes do not show any appreciable change. This qualitative observation is further confirmed in Table 1, where there is not a clear tendency in either of the chirp lifetimes. However, the slope of the instantaneous frequency clearly decreases as the pump power increases. This behavior replicates the theoretical results previously found by Ding and co-workers, as the reader can confirm in comparison with Fig. (3) of Ref. [12]. On the other hand, the noise present in the instantaneous frequency profiles is related with the measurement technique [14,15]. In the final step, it is necessary to divide by the temporal intensity profile of the pulse under test, whose instantaneous frequency will be measured, see Eq. (2) of Ref. [14]. A higher averaging during the temporal intensity profile recording reduces this noise, but simultaneously reduces the possibility to observe the fast details of each single pulse, therefore a trade-off between both must be reached. In addition, since the oscilloscope was triggered in the leading edge, the instantaneous frequency measurements on the falling edge are noisier.

In Ref. [11], we found that as the absolute value of the net-normal dispersion within the laser cavity is increased from 0.022 to 0.21 ps^2, the typical square-shaped DSR pulse [shown in Fig. 2(a)] transforms to a single right-angle trapezoid-shaped pulse. Further increments in dispersion (≥ 0.262 ps^2) generates multiple right-angle trapezoid-shaped pulses per round trip. Thus, we found it interesting to study the instantaneous frequency profile of these right-angle trapezoid-shaped pulses in order to compare with the previously discussed results. The setup used to measure the instantaneous frequency profile of

these pulses is the same used before and depicted in Fig. 1 with a dispersion line of 90 m long. Simultaneously, a 7.2 m long PM 980-XP optical fiber was added within the initial configuration of the laser cavity (Nufern, cutoff wavelength of 920 ± 50 nm, and numerical aperture of 0.120) with the purpose to generate these trapezoid-shaped DSR light pulses. Thus, the net dispersion grows up to 0.187 ps^2 remaining normal. There is a noticeable change in the temporal profile of the output light pulses from the original square-shaped to trapezium-shaped light pulse, see Fig. 4(a) as compared with Fig. 2(a). Now, across each single light pulse, the temporal intensity is no longer nearly constant, but clearly decreases from the leading to the trailing edge. Figure 4(a) also shows the dispersed input pulse after propagation by the 90 m long optical fiber. With both temporal intensity profiles, the instantaneous frequency is recovered according to the procedure developed in Refs. [14,15]. Figure 4(b) shows both the instantaneous frequency profile recovered by the dispersion technique as well as its corresponding fitting according to Eq. (2) for a fixed pump power of 577 mW. There is not a noticeable change in the qualitative features of the instantaneous frequency profile as compared with the results previously shown for the more common square-shaped flat-top DSR light pulse, i.e., in comparison with Fig. 2(b). Again, there is a nonzero linear frequency chirp across the pulse profile (2 GHz/ps) as well as an exponential chirp at the edges (10 and 11 ps for the leading and trailing chirp lifetimes, respectively). Both leading and trailing lifetime chirps have practically the same values as compared with our previous results, although now the pulse is approximately three times longer.

Figure 5 shows the measured instantaneous frequency profiles for this second DSR regime for the pump power in the range 338–577 mW. The lower limit represents the pump power threshold for self-started mode locking. The upper value is limited by the capability of our pump source. The main parameters of fitting according to Eq. (2), linear chirp slope, leading and trailing chirp lifetimes, are shown in Table 2 (for clarity, the curves corresponding to these fittings are not shown in Fig. 5). In Fig. 5, it can be observed that only the linear frequency chirp across the pulse profile changes as the
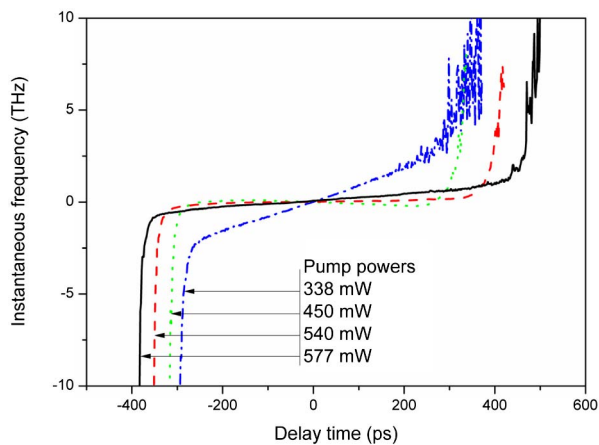
Table 1. Chirp Fitting Parameters for Square-Shaped DSR Light Pulses as a Function of the Pump Power

Pump Power (mW)	T_t (ps)	T_l (ps)	k (GHz/ps)
293	8.9 ± 0.4	4.2 ± 0.1	13 ± 1
375	11.2 ± 0.4	3.5 ± 0.1	14 ± 2
425	10.9 ± 0.5	3.9 ± 0.1	11 ± 2
467	10.8 ± 0.4	4.1 ± 0.1	8 ± 2
508	10.4 ± 0.2	4.0 ± 0.2	9 ± 1
583	10.3 ± 0.2	6.0 ± 0.3	5 ± 1

Fig. 5. Measured instantaneous frequency profiles for different pump powers for the trapezoid-shaped DSR emission.

Table 2. Chirp Fitting Parameters for Trapezoid-Shaped DSR Light Pulses as a Function of the Pump Power

Pump Power (mW)	T_l (ps)	T_t (ps)	k (GHz/ps)
338	9.3 ± 0.3	64 ± 7	8 ± 1
450	9.6 ± 0.5	12 ± 1	0 ± 1
540	10.4 ± 0.4	10 ± 1	1.1 ± 0.1
577	9.7 ± 0.5	11 ± 1	2.3 ± 0.1

pump power varies. On the other hand, leading and trailing chirp lifetimes do not show any appreciable change. This qualitative observation is further confirmed in Table 2, where there is not a clear tendency in either instantaneous frequency lifetimes (due to the high noise content, the high value of the trailing chirp lifetime at the lower pump power can be discarded). As opposed to the previous case of standard square-shaped DSR light pulses, in this case our measurements do not show a clear tendency for the linear chirp slope across the pulse as a function of the pump power. Although, it is clear from Fig. 4(a) that trapezoid-shaped pulses show less broadening effects as a consequence of dispersion. Therefore, a low linear chirp across the pulse is expected, which is confirmed in Table 2.

Finally, it is worthwhile to compare these results for a fixed pump power and different net-normal dispersion, which is equivalent to a fixed gain in a theoretical model. Figure 6(a) shows both intensity profiles for a pump power approximately equal (577 and 583 mW) but under different net-normal dispersions (0.008 and 0.187 ps², respectively). At the same pump power, the DSR light pulse generated under higher net-normal dispersion is considerably longer, following the same trend theoretically predicted in Ref. [12]. Figure 6(b) shows the respective instantaneous frequency profiles, the DSR generated under higher net-normal dispersion presents the lower linear chirp, which again is in accordance with the theoretical results of Ref. [12].

In conclusion, in this work we provide a detailed experimental characterization of the instantaneous frequency profile of
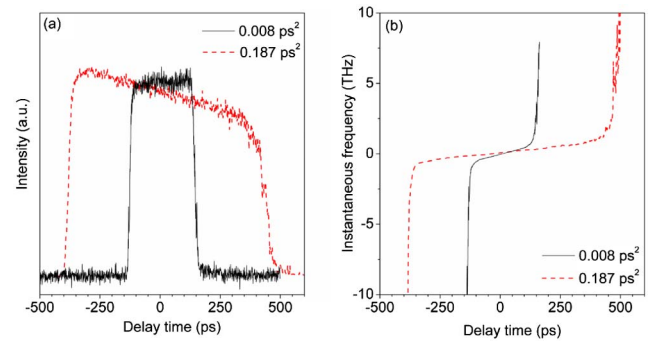

Fig. 6. Comparison at a constant pump power of ∼580 mW and different net-normal dispersions: (a) temporal intensity profiles and (b) instantaneous frequency profiles.

DSR pulses. The measurements have been done using a technique well suited for relatively long pulses. Our results show good agreement with theoretical predictions and provide outstanding information to confirm the theory of DSR light pulses.

REFERENCES

1. N. Akhmediev, J. M. Soto-Crespo, and P. Grelu, Phys. Lett. A **372**, 3124 (2008).
2. W. Chang, A. Ankiewicz, J. M. Soto-Crespo, and N. Akhmediev, Phys. Rev. A **78**, 023830 (2008).
3. P. Grelu, W. Chang, A. Ankiewicz, J. M. Soto-Crespo, and N. Akhmediev, J. Opt. Soc. Am. B **27**, 2336 (2010).
4. X. Liu, Phys. Rev. A **81**, 053819 (2010).
5. X. Zhang, C. Gu, G. Chen, B. Sun, L. Xu, A. Wang, and H. Ming, Opt. Lett. **37**, 1334 (2012).
6. Z.-C. Luo, W.-J. Cao, Z.-B. Lin, Z.-R. Cai, A.-P. Luo, and W.-C. Xu, Opt. Lett. **37**, 4777 (2012).
7. L. Liu, J. H. Liao, Q. Y. Ning, W. Yu, A.-P. Luo, S.-H. Xu, Z.-C. Luo, Z.-M. Yang, and W.-C. Xu, Opt. Express **21**, 27087 (2013).
8. J. H. Yang, C. Y. Guo, S. C. Ruan, D. Q. Ouyang, H. Q. Lin, Y. M. Wu, and R. H. Wen, IEEE Photon. J. **5**, 1500806 (2013).
9. L. Mei, G. Chen, L. Xu, X. Zhang, C. Gu, B. Sun, and A. Wang, Opt. Lett. **39**, 3235 (2014).
10. K. Krzempek, Opt. Express **23**, 30651 (2015).
11. I. Armas-Rivera, C. Cuadrado-Laborde, A. Carrascosa, E. A. Kuzin, G. Beltrán-Pérez, A. Díez, and M. V. Andrés, Opt. Express **24**, 9966 (2016).
12. E. Ding, P. Grelu, and J. N. Kutz, Opt. Lett. **36**, 1146 (2011).
13. D. Li, L. Li, J. Zhou, L. Zhao, D. Tang, and D. Shen, Sci. Rep. **6**, 23631 (2016).
14. C. Cuadrado-Laborde, A. Carrascosa, P. Pérez-Millán, A. Díez, J. L. Cruz, and M. V. Andres, Opt. Lett. **39**, 598 (2014).
15. C. Cuadrado-Laborde, M. Brotons-Gisbert, G. Serafino, A. Bogoni, P. Pérez-Millán, and M. V. Andrés, Appl. Phys. B **117**, 1173 (2014).
16. G. P. Agrawal, *Nonlinear Fiber Optics* (Academic, 2001), p. 72.